Pilot test and optimization of plasma based deNOx

Stamate, Eugen; Chen, Weifeng; Michelsen, Poul

Publication date:
2009

Document Version
Publisher's PDF, also known as Version of record

Pilot test and optimization of plasma based deNOx

Risø-R-Report

Eugen Stamate, Weifeng Chen and Poul Kerff Michelsen
Risø-R-1689(EN)
April 2009

Risø DTU
National Laboratory for Sustainable Energy

Authors: Eugen Stamate, Weifeng Chen and Poul Kerff Michelsen
Title: Pilot test and optimization of plasma based NOx reduction
Division: Plasma Physics and Technology Programme

Risø-R-1689(EN)
April 2009

Abstract:

The NO_x reduction of flue gas by plasma generated ozone was investigated in pilot test experiments at two industrial power plants running on natural gas (Ringsted) and biomass (Haslev). Reduction rates higher than 95% have been achieved for a molar ratio O_3:NO_x of 1.56. Fourier transform infrared and ultraviolet absorption spectroscopy were used for spatial measurements of stable molecules and radicals along the reduction reactor. Reactions of O_3 injected in the flue gas in the reduction reactor were also modeled including the influence of the flue gas temperature, water droplets and SO_x and HCl content. Experiments are in good agreement with numerical simulations. An optimized oxidation scheme for NO_x reduction processes with time dependent combustion, such as the biomass power plants, was developed. Ozone production by micro-hollow and capillary discharges at atmospheric pressures was investigated for oxygen and air gas flows.

ISSN 0106-2840
ISBN 978-87-550-3744-1

Contract no.:

PSO: 2006-1-6365

Group's own reg. no.:
1710047-1

Sponsorship:

Cover :

Pages: 31
Tables: 2
References: 21

Information Service Department
Risø National Laboratory for Sustainable Energy
Technical University of Denmark
P.O.Box 49
DK-4000 Roskilde
Denmark
Telephone +45 46774004
bibl@risoe.dk
Fax +45 46774013
www.risoe.dtu.dk

Contents

Preface

This report summarizes the work performed by Risø DTU for the PSO project no. 2006-1-6365 “Pilot test and optimization of plasma based NOx reduction”.

The project was carried out in collaboration between Risø National Laboratory for Sustainable Energy, Technical University of Denmark (Risø DTU), the Danish Gas Technology Centre (DGC) and DONG Energy over a three year period (March 2006-February 2009). Laboratory experiments on NO_x reduction and ozone optimization were carried at DGC in collaboration with Risø DTU. The pilot test experiments were carried out at the power plant running on natural gas in Ringsted and at the power plant running on biomass in Haslev.

The authors express their gratitude to Dr. Alexander Fateev for direct support and to Dr. B. Stenum†, Dr. H. Mortensen, Dr. Y. Kusano, Dr. F. Leipold and Dr. H. Bindslev for their early involvement in this research.

1 Summary

The aim of the project was to,

- Scale-up of the plasma based NO_x reduction to pilot scale and test it in a natural gas engine power plant and a biomass power plant;
- Investigate the influence of the additional constituents of flue gas coming from biomass combustion (HCl and SO_2) and their reaction products collected in the scrubber;
- Develop a chemical kinetics model of plasma based NO_x reduction;
- Optimise the ozone production using plasma discharges at atmospheric pressure.

All project objectives have been successfully addressed in a very good collaboration between DONG Energy, DGC and Risø DTU. Risø DTU's effort was mainly concentrated on process diagnostics by UV and FTIR during the pilot test measurements, chemical kinetics modelling of the NO_x reduction process and ozone production optimization.

FTIR and UV gas absorption measurements have been performed during the NO_x reduction process both at Ringsted (natural gas power plant) and Haslev (biomass power plant). Reduction rates higher than 95% have been achieved for a molar ratio O_3:NO_x = 1.56 for the natural gas plant. A rate equation model has been developed to assess the chemical kinetics for the NO_x process in the reactor under various experimental conditions (for example, different flue gas temperatures and humidity). A good agreement was found between measured and calculated values of the main species. Simulation suggests that in current experiment conditions, the deNO_x efficiency is highest for a flue gas temperature of 100 ^oC. The addition of small water spray droplets in the reactor may further improve the NO_x oxidation rate. Due to combustion particularities in the biomass power plant the NO_x level exhibited very large variation within time intervals of less than a minute. An optimized reduction scheme that can significantly improve the ozone consumption in a time dependent process has been developed and partially implemented. Kinetic simulations show that SO_2 oxidation by ozone is too low and that HCl and SO_x are not affecting the NO_x reduction rate. It was shown that fine water droplets of a few tens of μm contribute significantly to N_2O_5 capture in the reactor. The ozone production by multi hollow and capillary discharges was investigated for different discharge parameters. The results show that a complex construction structure including thick metallic films deposited on dielectric materials is necessary for long and steady operation of these discharges.

2 Pilot test measurements in a power plant running on natural gas

2.1 Introduction

Nitrogen oxides (NO_x = NO + NO_2) formed during fuel burning affect the quality of air, soil and water through acid rains. At higher concentrations they may also have a direct negative influence on human health [1]. Recent environmental concerns lead to stringent regulations on the allowed levels of NO_x emission from combustion power plants, gas turbines, incinerators, boilers, diesel engines and other polluting sources. Available technologies for NO_x reduction includes: selective catalytic reduction [2], selective non-catalytic reduction [3, 4], low-temperature oxidation by ozone [5], non-thermal plasma [6-9], electron beam irradiation and several hybrid techniques [10, 11]. Despite of this variety, none of these methods is free of trade-offs and limitations including capital investments and/or operational costs. Low temperature oxidation (LTO) of NO_x by ozone (O_3) injection is an attractive gas cleaning process where the relatively insoluble NO_x is oxidized to higher oxides such us N_2O_5 that are highly soluble and can easily be removed in wet scrubbers [5, 12]. NO_x oxidation method by ozone injection has several advantages compared to other deNO_x techniques, as e.g. direct ozone production in the reactor, because the plasma discharge is kept clean and the removal rate of NO is higher than direct oxidation methods where the reverse reactions occur to reform NO and NO_2 by O radical. [13, 14] Despite of these advantages the low-temperature oxidation technique is still relatively expensive, a fact that requires further process optimization and cost estimation for the whole deNO_x reduction process. There are only few reports in the literature on NO_x reduction experiments on industrial power plants using the LTO technique [15]. Therefore, detailed online measurements of the spatial NO_x and ozone concentration profiles along an LTO oxidation reactor will be beneficial for a deeper understanding of the chemical kinetics in order to design an efficient deNO_x reactor for practical application of LTO technique in industry.

2.2 Experimental details - Ringsted

The movable measurement stand realized and tested at Risø DTU to collect UV and FTIR data at different port along the reactor is presented in Fig. 1 (a) located at Risø DTU, (b) placed under the reactor inside of the container, (c) including placement details for the optical tables supporting the UV and FTIR equipment.

(a)

(b)

(c)

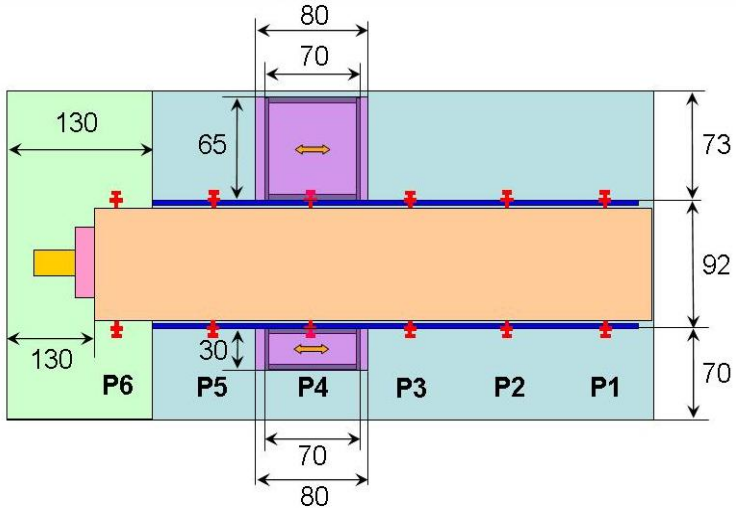

Fig. 1 (a) Movable stand used for UV and FTIR measurements build and tested at Risø DTU; (b) The movable measurement stand placed under the rector inside of container; (c) Emplacement of the measurements parts near the reactor.

The flue gas source located in Ringsted is a 2×5.5 MW_{el} natural gas fired power plant with a total flow rate of the flue gas of 49000 Nm^3/h from which only a portion of 3% was treated for NO_x reduction. The flue gas temperature was steady at 60 ^oC. The main component of NO_x in the flue gas was NO (over 90%) and the total NO_x level was kept by process optimization at around 80 ppm. Fig. 2 shows a schematic of the experimental setup. A 4.5 m long and 0.6 m in diameter reactor with a

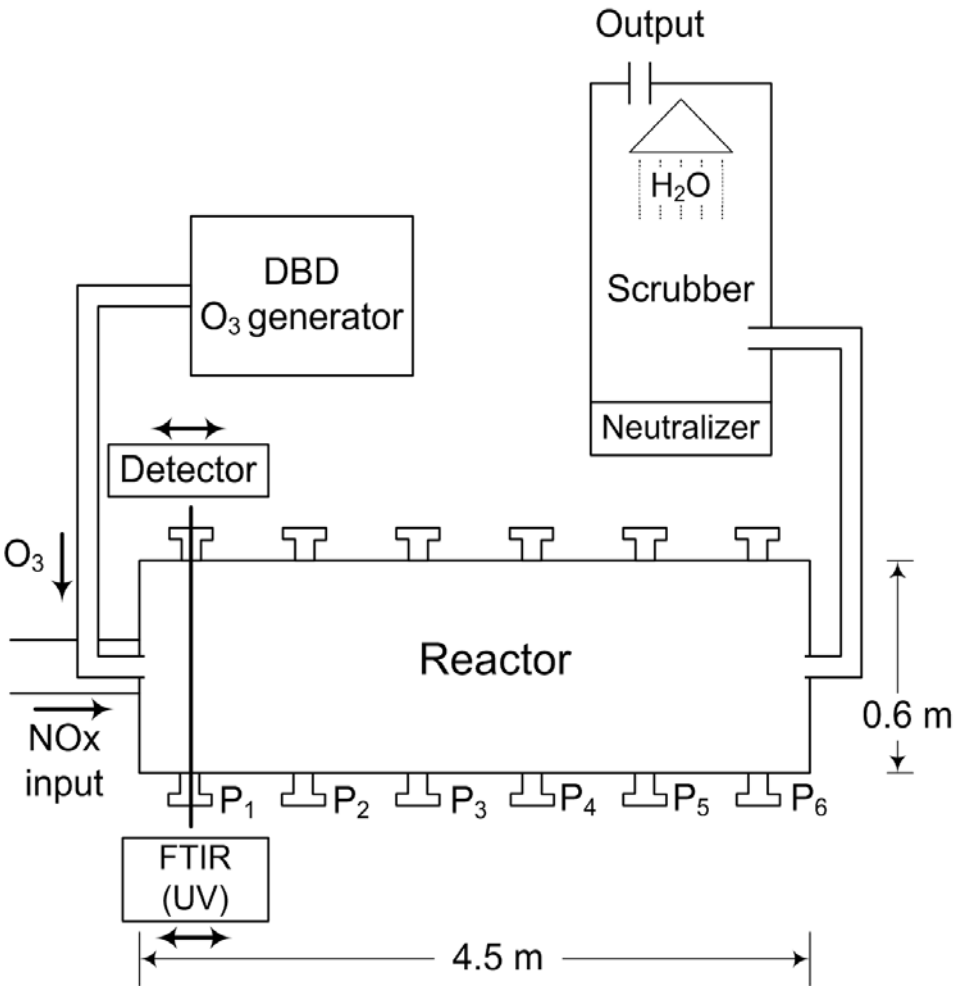

Fig. 2 Schematic of the NO_x oxidation process using ozone.

residence time of the flue gas of about 5 seconds was used to oxidize the NO_x to soluble N_2O_5. Ozone produced by a Wedeco® generator based on dielectric barrier discharge plasma source operated in O_2 was injected into the reactor and mixed with the flue gas. A wet scrubber unit was used to capture and neutralize the N_2O_5 before releasing the treated gas in the atmosphere. To evaluate the NO_x removal efficiency, the input (before the oxidation reactor) and output (after the wet scrubber), NO_x concentrations have been measured by a chemiluminescence analyzer (CLD60, Eco

Physics). O_3, NO_2, N_2O_5 and HNO_3 in the reactor were measured by FTIR (MB-100, BOMEM) spectrometer. Ozone concentration was also measured by UV absorption at 254 nm. Six equidistant observation ports (0.87 m) along the reactor were used to detect IR and UV absorption signals. The measurement equipment was placed on a table movable under the reactor, thus keeping the same optical alignment. The following six concentrations of ozone injected into the reactor were used: 1) 25 ppm; 2) 50 ppm; 3) 75 ppm; 4) 100 ppm; 5) 125 ppm; and 6) 150 ppm.

2.3 Chemical mechanism of O_3-NO_x

Processes influencing on the NOx oxidation in the flue gas after the ozone injection were modeled using the chemical kinetics simulation program *CHEMSIMUL*. [16] The program principally consists of a solver of ordinary differential equation (ODE) systems with additional code to transform chemical reaction schemes to ODEs.

2.4 Gas phase reactions

Table 1 lists the gas phase reactions included in the model along with the rate constant parameters used in the program. The reaction rate constants are calculated as

$$k = AT^{\beta}\,\mathrm{e}^{-\frac{E_a}{RT}}, \qquad (1)$$

where R=1.987207× 10^{-3} kcal × mol^{-1} × K^{-1} is the gas constant, E_a is the activation energy (kcal × mol^{-1}), β is an empirical constant, and T is the gas temperature. Most of the rate constants in the Table 1 were obtained from the National Institute for Standards and Technology (NIST) kinetic database [17]. In the simulation, all reactions must be treated as bimolecular. For three-body reactions this was achieved by assuming a constant third body density corresponding to an ideal gas at 1 atm., room temperature. In reaction R30, however, the third body concentration was assumed to equal the initial concentration of [H_2O]. The rate constant of R31 was estimated by an extrapolation from those of R19 and R30 based on the equidistance of the activation energies as calculated by Voegele et al. [18].

ID	Reaction	A (cm^3 $molecule^{-1}s^{-1}$)	E_a (kcal/mol)	β	Ref
R1	$NO + O_3 \rightarrow NO_2 + O_2$;	3.16×10^{-12}	3.1	0	[1]
R2	$NO_2 + O_3 \rightarrow NO_3 + O_2$;	1.20×10^{-13}	4.87	0	[1]
R3	$NO_2 + NO_3 \rightarrow N_2O_5$;	9.42	0	-4.5	[1]
R4	$O_3 + N_2 \rightarrow O_2 + O(^3P) + N_2$;	7.16×10^{-10}	22.26	0	[1]
R5	$O(^3P) + O_3 \rightarrow 2\ O_2$;	3.11×10^{-14}	3.14	0.75	[1]
R6	$O(^3P) + O_2 \rightarrow O_3$;	2.32×10^{-9}	0	-2.2	[1]
R7	$N_2O_5 + N_2 \rightarrow NO_2 + NO_3 + N_2$;	4.57×10^{5}	21.86	-3.5	[1]
R8	$NO_3 \rightarrow NO + O_2$;	2.50×10^{6}	12.12	0	[1]
R9	$NO + O(^3P) \rightarrow NO_2$;	1.51×10^{-6}	0	-2.41	[1]
R10	$NO_2 + O(^3P) \rightarrow NO_3$;	271	2.29	-4.94	[1]
R11	$NO_3 + O(^3P) \rightarrow O_2 + NO_2$;	1.00×10^{-11}	0	0	[1]
R12	$2\ NO_3 \rightarrow O_2 + 2\ NO_2$;	8.50×10^{-13}	4.87	0	[1]
R13	$NO_2 + NO_3 \rightarrow O_2 + NO + NO_2$;	5.40×10^{-14}	2.96	0	[1]
R14	$2\ NO_2 \rightarrow O_2 + 2\ NO$;	2.71×10^{-12}	26.03	0	[1]
R15	$2\ NO_2 \rightarrow NO + NO_3$;	1.59×10^{-14}	20.87	0.73	[1]
R16	$2\ NO_2 \rightarrow N_2O_4$;	0.0259	0	-4.8	[1]
R17	$N_2O_4 + H_2O \rightarrow HNO_3 + HNO_2$;	4.18×10^{-10}	11.59	0	[1]
R18	$N_2O_4 + N_2 \rightarrow 2\ NO_2 + N_2$;	3.28×10^{4}	12.72	-3.8	[1]
R19	$N_2O_5 + H_2O \rightarrow 2\ HNO_3$;	2.51×10^{-22}	0	0	[1]
R20	$HNO_2 + NO_3 \rightarrow HNO_3 + NO_2$;	1.00×10^{-15}	0	0	[1]
R21	$NO_3 + NO \rightarrow 2\ NO_2$;	1.80×10^{-11}	-0.22	0	[1]
R22	$O_3 + NO_2 \rightarrow NO + 2\ O_2$;	1.00×10^{-18}	0	0	[1]
R23	$O_3 + NO_3 \rightarrow NO_2 + 2\ O_2$;	1.00×10^{-17}	0	0	[1]
R24	$NO + NO_3 \rightarrow 2\ NO + O_2$;	2.71×10^{-11}	1.882	-0.23	[1]
R25	$2\ O(^3P) \rightarrow O_2$;	3.82×10^{-13}	-1.79	-1	[2]
R26	$O(^3P) + NO_2 \rightarrow O_2 + NO$;	5.5×10^{-12}	0.3736		[2]
R27	$2\ NO + O_2 \rightarrow 2\ NO_2$;	5.61×10^{-21}	1.053		[2]
R28	$NO + NO_2 \rightarrow N_2O_3$;	2.70×10^{7}	0	-8.7	[2]
R29	$N_2O_3 + N_2 \rightarrow NO + NO_2 + N_2$;	6.76×10^{14}	9.7	-8.7	[2]
R30	$N_2O_5 + 2\ H_2O \rightarrow 2\ HNO_3 + H_2O$;	4.4×10^{-21} (*)			
R31	$N_2O_5 + 3\ H_2O \rightarrow 2\ HNO_3 + 2\ H_2O$;	8×10^{-20} (**)			

(*) Termolecular reaction; (**) Quadrimolecular reaction.

Table 1. Detailed O_3 - NO_x reaction mechanism.

2.5 Heterophase reactions

Three additional, heterophase reactions were included in the model to account for the decomposition of oxygen atoms and ozone on the reaction walls and a possible hydrolysis of N_2O_5 on any water-containing particles in the flue gas.

Reaction R32:

$$\frac{\mathrm{d}[\mathrm{O}(^3P)]}{\mathrm{d}t} = -[\mathrm{O}(^3P)]\left(\frac{(30\,\mathrm{cm})^2}{5.78\times 0.292\,\mathrm{cm^2 s^{-1}}(T/273\,\mathrm{K})^{1.5}} + \frac{2\times 30\,\mathrm{cm}}{9.9\times 10^{-3}\sqrt{2}\times 4.25\times 10^4\ \mathrm{cm\,s^{-1}}\sqrt{T/273\,\mathrm{K}}}\right)^{-1} \quad (2)$$

Reaction R33:

$$\frac{\mathrm{d}[\mathrm{O}_3]}{\mathrm{d}t} = -[\mathrm{O}_3]\left(\frac{(30\,\mathrm{cm})^2}{5.78\times 0.208\,\mathrm{cm^2 s^{-1}}(T/273\,\mathrm{K})^{1.57}} + \frac{2\times 30\,\mathrm{cm}}{2\times 10^{-6}\sqrt{2}\times 3.47\times 10^4\ \mathrm{cm\,s^{-1}}\sqrt{T/273\,\mathrm{K}}}\right)^{-1} \quad (3)$$

2.6 Hydrolysis of N_2O_5 on droplets

NO_2 can be reproduced by $N_2O_5 \rightarrow NO_2 + NO_3$ back reaction (reaction R7). However this reaction can be suppressed in the presence of a sink for N_2O_5 molecules. One possible sink can be the water droplets from condensation in the reactor. The N_2O_5 uptake by water droplets has been studied by Van Doren *et al.* [19]. They expressed the rate of uptake in terms of an uptake coefficient, γ_{obs}, which based on their measurements, can be roughly extrapolated to a value of 0.02 for N_2O_5 into water. This coefficient is related to the flux of N_2O_5 into water droplets by $J = n_g \bar{c}\gamma_{obs}/4$, where n_g is the gas density ($[N_2O_5]$) and $\bar{c} = \sqrt{3RT/M_{N_2O_5}} \approx 300\,\mathrm{m/s}$ is the root mean square thermal velocity of the N_2O_5 molecules, which have a molar mass of $M_{N_2O_5} = 0.108\,\mathrm{kg/mol}$. Let us assume, for example, that a fraction x of the H_2O has condensed and, for simplicity, that spherical droplets of equal radius, r are formed. The number density of such droplets is $n_d = n_c/N_d$, where n_c is the number density of water molecules that have been condensed into the droplets:

$$n_c = x\cdot[\mathrm{H_2O}] = x\cdot C_{\mathrm{H_2O}}\cdot\frac{p}{k_B T}, \quad (4)$$

and N_d is the number of molecules in each such droplet:

$$N_{\mathrm{d}} = \frac{N_{\mathrm{A}} m_{\mathrm{d}}}{M_{\mathrm{H_2O}}} = \frac{4 N_{\mathrm{A}} \rho \pi r^3}{3 M_{\mathrm{H_2O}}}, \tag{5}$$

with $\rho \approx 1$ g/cm^3 the density of water, $M_{\mathrm{H_2O}} = 18\,\mathrm{g/mol}$ its molar mass, and N_A Avogadro's number.

The overall rate of N_2O_5 uptake by these droplets is given by Reaction R34: $-\mathrm{d}[\mathrm{N_2O_5}]/\mathrm{d}t = JA \equiv \nu_u [\mathrm{N_2O_5}]$, where A is the total surface area of droplets per unit of vessel volume:

$$A = 4\pi r^2 n_{\mathrm{d}} = \frac{3x \cdot C_{\mathrm{H_2O}} \cdot pM_{\mathrm{H_2O}}}{\rho r R T}. \tag{6}$$

Inserting the above values, C_{H2O}=10%, and p=1 atm, a value for the uptake frequency ν_u of ~ 0.3 s^{-1} is found for r = 100 μm and ~3 s^{-1} for r = 10 μm. In the present study simulations were performed for both cases: without water droplets and with water droplets of these two drop radii.

2.7 Results and discussion

Calculated evolutions of O_3, NO, NO_2, and N_2O_5 concentrations in the reactor during 5 seconds after ozone injection are shown in Fig. 3 as an example, at (a) 75 ppm ozone input and (b) 150 ppm ozone input. The kinetic curves in the Fig. 2 were calculated for the NO initial concentration of 73 ppm and the NO_2 initial concentration of 7 ppm. The simulations in the Fig. 3 do not include any effect of heterophase reactions (Reaction R32, R33, R34). One can see that immediately after ozone injection, the concentration of NO decreases and the concentration of NO_2 increases accordingly. This is due to the fast reaction

$$\text{Reaction R1:} \qquad \mathrm{NO + O_3 \rightarrow NO_2 + O_2}, \tag{7}$$

Characteristic time of the NO conversion to NO_2 depends on the O_3 concentration. Therefore, the first main path of NO_x reduction is the rapid oxidation of NO to NO_2 and, later conversion to the N_2O_5 through reactions (8-9) takes place,

Reaction R2: $NO_2 + O_3 \rightarrow NO_3 + O_2$, and (8)

Reaction R3: $NO_2 + NO_3 + M \rightarrow N_2O_5 + M$. (9)

The slower process R2 takes place after the process R1 is completed. So, when the input ozone concentration is less than NO concentration, in the first stage the ozone is consumed in $NO \rightarrow NO_2$ conversion without remarkable decrease in $NO+NO_2$

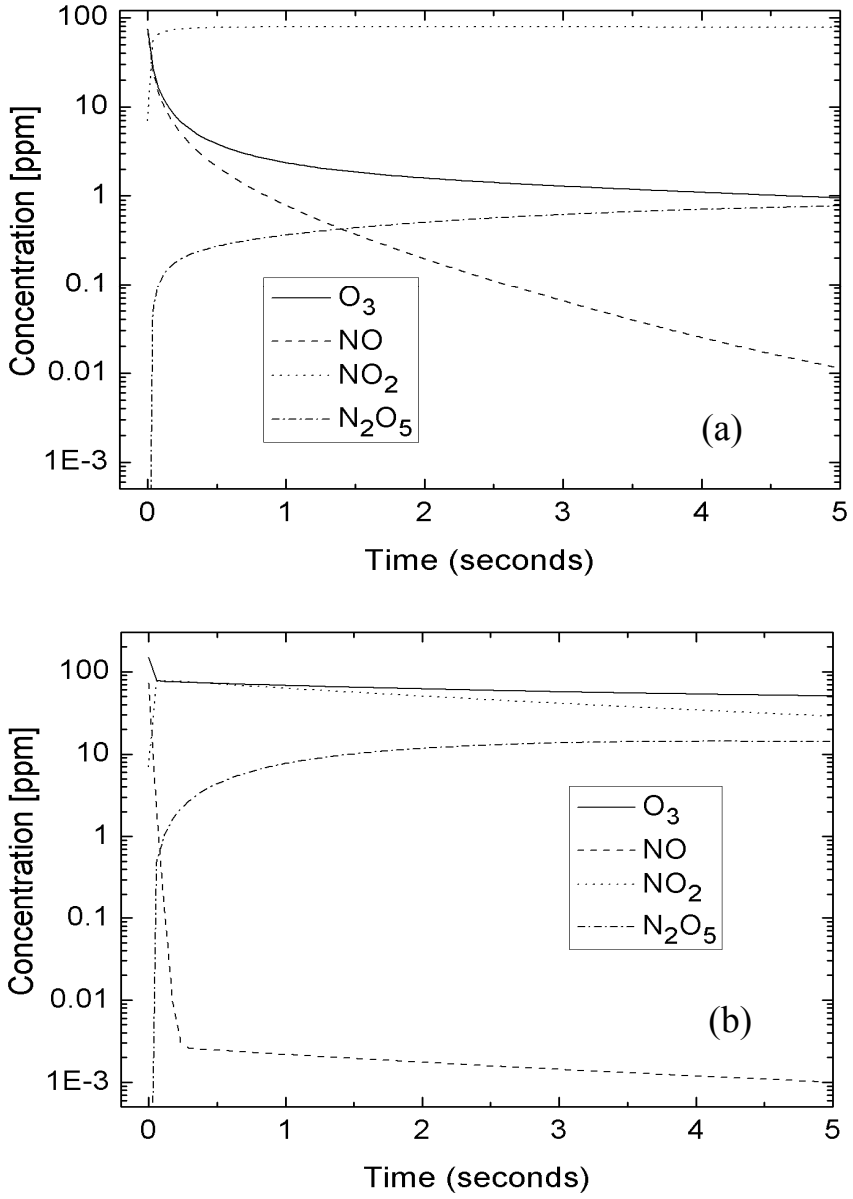

Fig. 3. Calculated evolutions of the concentrations of O_3, NO, NO_2, N_2O_5 in the reactor during 5 seconds after ozone injection without considering any effects of heterophase reactions (a) 75 ppm ozone input, (b) 150 ppm ozone input.

concentration as shown in Fig. 3 (a). At higher ozone input level (150 ppm), the conversion of NO to NO_2 is rapid (t < 0.3 seconds) and the excess ozone is used to further oxidize NO_2 (Reaction R2, R3).

The characteristic time of the reaction R2 is determined by the O_3 concentration, as well as the NO_2 concentration determined by reaction R1. For a case when all NO_x is NO, one can get a deNO_x reaction path from reactions R1, R2 and R3,

$$\text{Reaction RA: } NO + 1.5\ O_3 \rightarrow 0.5\ N_2O_5 + 1.5\ O_2. \quad (10)$$

However, when NO_x is 100 percent by NO_2, one can get a deNO_x reaction path from Reaction R2 and R3,

$$\text{Reaction RB: } NO_2 + 0.5\ O_3 \rightarrow 0.5\ N_2O_5 + 0.5\ O_2. \quad (11)$$

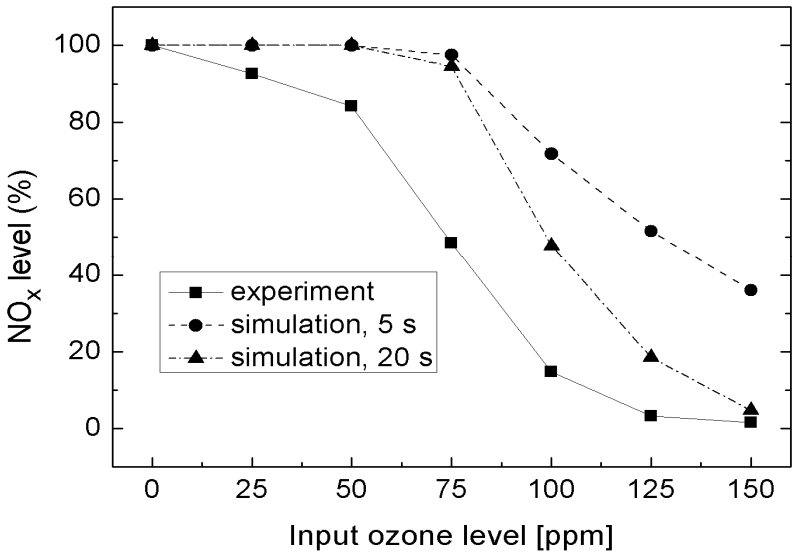

Fig.4 Remained NO_x after the scrubber at different input ozone level by both experiment measurement and simulations for a residence time of 5 and 20 sec.

This means that if NO is the main component in NO_x, to remove one NO molecule, 1.5 O_3 molecules are needed, and in the case when NO_2 is the main component in NO_x, 0.5 O_3 molecules are needed to remove one NO_2 molecule.

Fig. 4 shows the remained NO_x level after the scrubber at various ozone input levels. The NO_x reduction efficiency reached 85% for 100 ppm O_3 (molar ratio

O_3:NOx = 1.25) and it was higher than 95 % for a 125 ppm input O_3 (molar ratio O_3:NO_x = 1.56). In this calculation a residence time of 5 s in the reactor and no wet

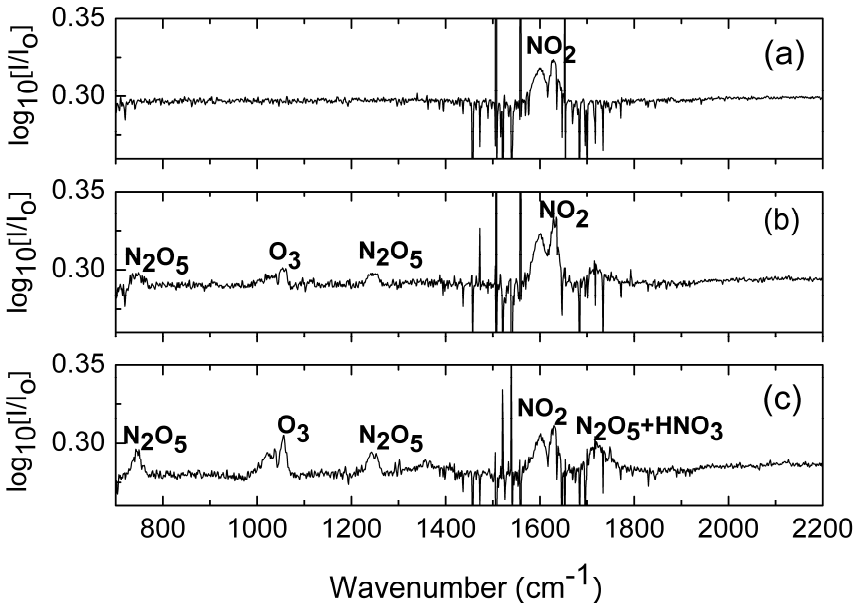

Fig. 5 FTIR absorption spectra measured at P_2 for (a) 25, (b) 100 and (c) 150 ppm ozone input.

scrubbing by water droplets have been assumed.

The spatial distribution of different species was measured by moving the measurement equipment to the various ports. Typical FTIR spectra measured at P_2 port for different ozone input concentrations are shown in Fig. 5. The overlap of water absorption band and NO limits NO detection by FTIR. While the ozone was quickly consumed at lower O_3 inputs (25 ppm and 50 ppm) where no O_3 could be detected by FTIR, the NO_2 peak was the dominant peak. For higher ozone input (150 ppm), O_3, NO_2, N_2O_5 and HNO_3 were all detected even after about 1 second (P_2) after the O_3 injection.

Remained ozone concentration at ports P_2 to P_5 as a function of the ozone input level measured by both FTIR and UV is shown in Fig. 6 for NO = 80 ppm. The NO_x removal process by ozone oxidation was modeled by solving the rate equations of chemical reactions as listed in the Table 1. Concentrations of different species as a function of the residence time were calculated. Remained ozone levels are shown with dashed lines in Fig. 6 for residence times corresponding to ports P_2 (1 s) and P_6 (5 s). From calculations, it can be see that for initial ozone concentrations below 80 ppm (O_3:$NO_x \leq 1$), all ozone is consumed for NO+NO_2 oxidation and no ozone remains in the reactor. In the measurements, ozone was

detected for input levels higher than 50 ppm, this may be due to incomplete reaction of ozone in the real situation. With further increase of ozone concentration, the amount of the ozone remained in the reactor increased, however with longer residence time (for example from 1 second or P_2 to 5 seconds or P_5) the concentration of the remained ozone decreased. Calculations and experimental

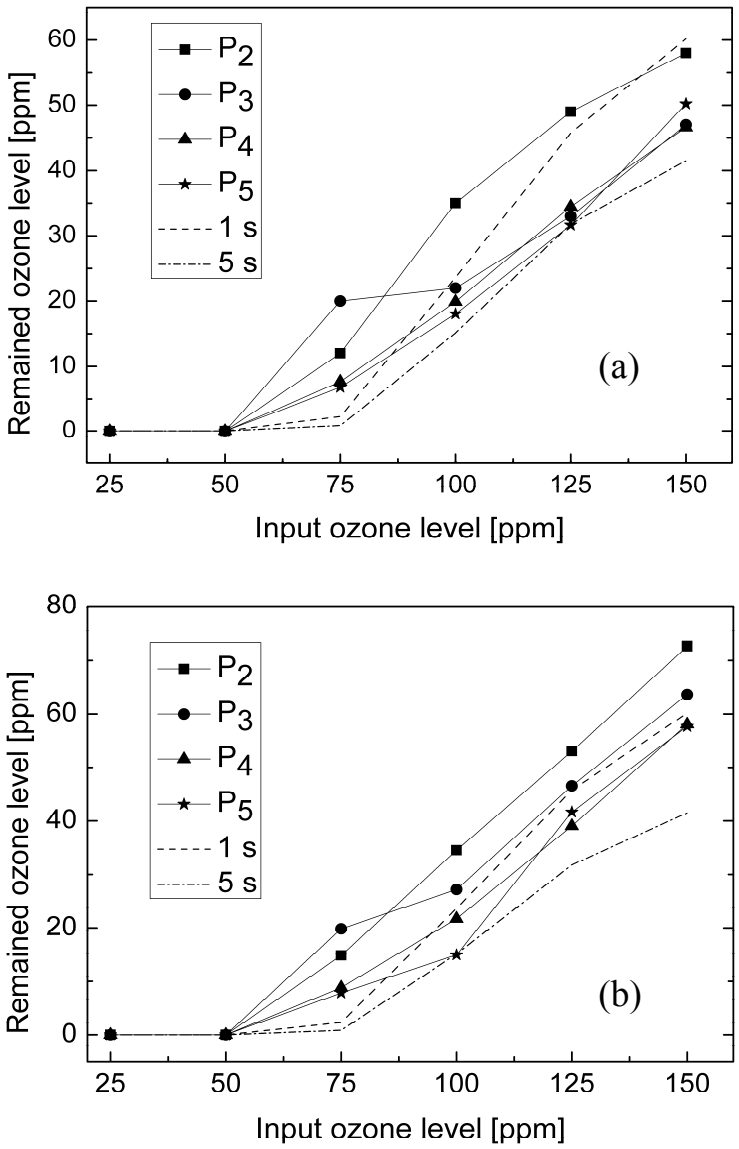

Fig. 6 Ozone concentrations at ports P_2-P_5 as a function of ozone input level measured by (a) FTIR and (b) UV absorption. Dashed lines show the simulated ozone concentration for a residence time of 1 and 5 sec, respectively where, NO=80 ppm and *T*= 60 °C.

results by both FTIR and UV absorption are in good agreement. To achieve high ozone utilization efficiency, long residence time of the flue gas in the reactor is desired. This can be achieved by uniform distribution of the ozone and adequate

mixing of ozone with flue gas and a longer reaction zone.

Simulated NO_2 and N_2O_5 values at different ozone input levels and time after ozone injection with no water sink effect and 10 μm water droplets in the reactor are shown in Figure 7. The NO_2 concentration increases with O_3 input

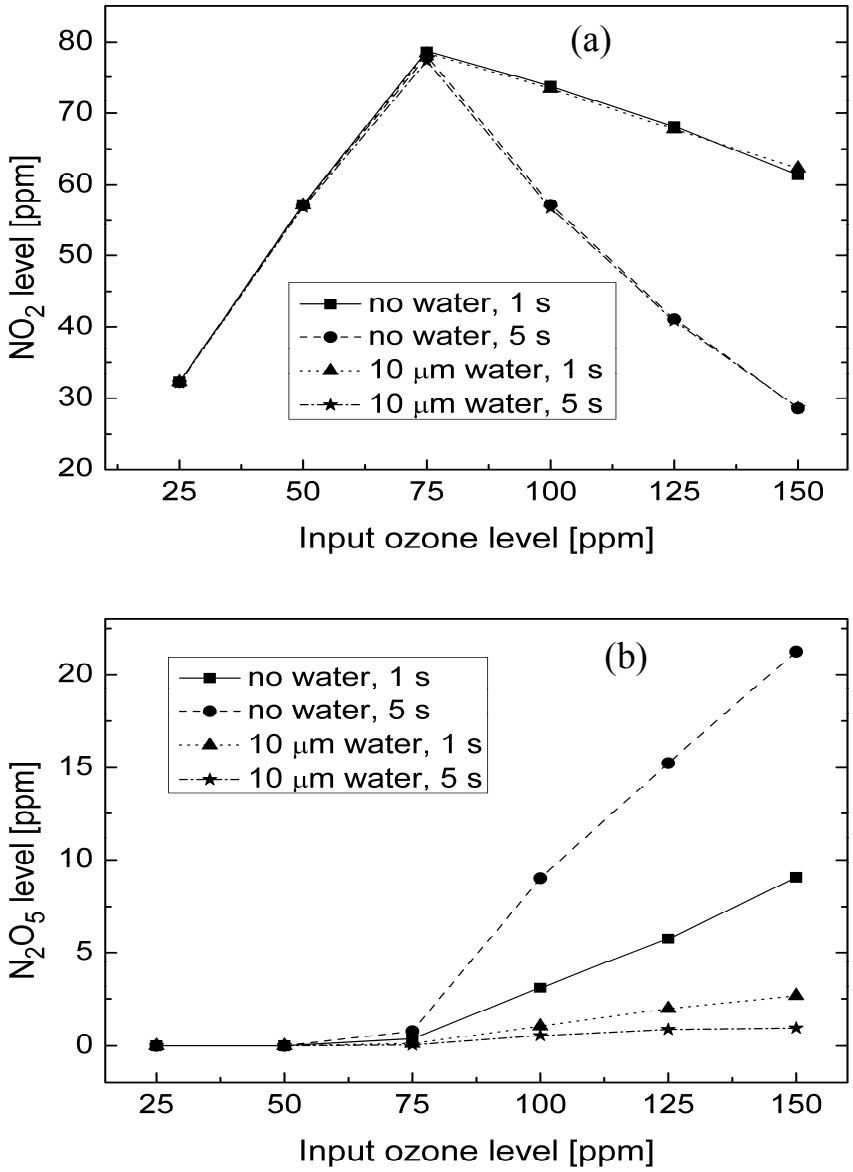

Fig. 7 Simulated NO_2 (a) and N_2O_5 (b) in case of no water in the reactor and 10 μm water droplets in the reactor for T=60 °C.

because of NO to NO_2 conversion at low O_3 input but it decreases for higher O_3 input due to NO_2 to N_2O_5 conversion. In the case of no water sink effect, the N_2O_5 concentration increases with O_3 input and also with the residence time in the reactor. Without considering water sink effect in simulation, the calculated values for N_2O_5 are, as expected, higher than the measured values. However, by taking into

consideration 10 μm water droplets in the reactor, the calculated values for N_2O_5 were much lower than the measured values. This suggests that small water droplets have a larger water sink effect on capturing the N_2O_5. Figure 8 presents the NO_2 (a)

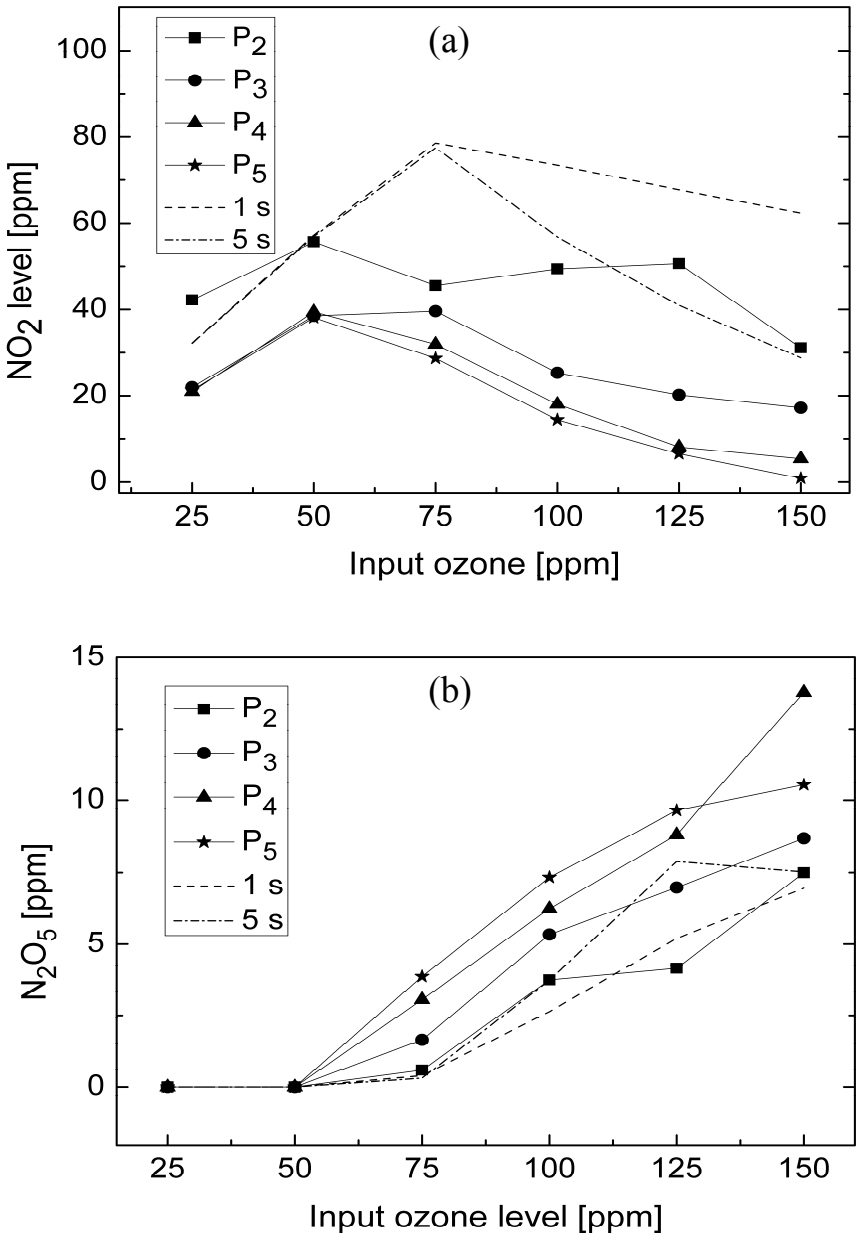

Fig. 8 NO_2 (a) and N_2O_5 (b) with simulation considering water sink (100 μm water droplets) effect for N_2O_5, where NO=80 ppm, T=60 °C.

and N_2O_5 (b) measured concentrations together with simulation considering water sink (100 μm water droplets) effect for N_2O_5. Compared with the case of no water sink effect or the case of 10 μm water droplets in the reactor as shown in the Fig. 7, the calculations in the Fig. 8 shows the best fit correlation with measured values.

It is also interesting to study the effects of flue gas temperature and water capture of N_2O_5 on deNO_x kinetics. Fig. 9 shows calculated concentrations of NO_2 (a), (a) and (e) and N_2O_5 (b), (d) and (f) without considering water sink effect (a) and (b), (c) and (d) considering 100 μm water droplets, and (e) and (f) considering 10 μm water

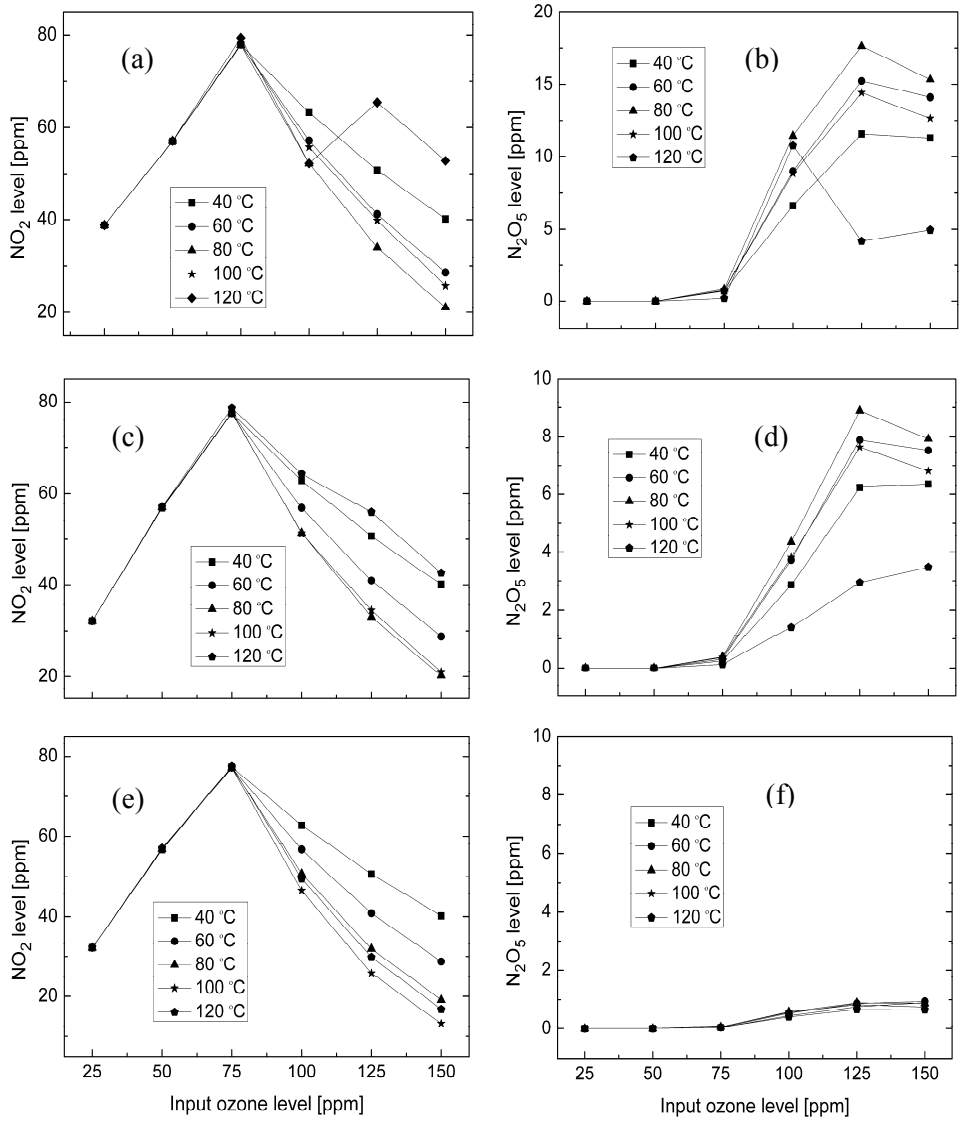

Fig. 9 Temperature dependent concentrations of NO_2 (a), (c) and (e) and N_2O_5 (b), (d) and (f) by calculations (a) and (b) without considering water sink effect for N_2O_5, (c) and (b) considering 100 μm water droplets and (e) and (f) considering 10 μm water droplets (residence time = 5 s, NO=80 ppm).

droplets for N_2O_5 removal at different temperatures within 5 seconds after ozone injection. It shows that in the cases of no water ((a) and (b)) or 100 μm water in the reactor ((c) and (d)), at 80 ^oC the NO_x removal efficiency is the highest (with smallest NO_2 concentration and highest N_2O_5 concentration). The optimum reduction temperature increases to 100 ^oC in the case considering 10 μm water droplets, Fig. 9

(e). The decomposition rate of ozone (reaction R4: $O_3 + N_2 \rightarrow O_2 + O(^3P) + N_2$) increases at high temperature (over 80 ^oC) and less ozone is used for NO_x oxidation. The decomposition of N_2O_5 (reaction R17: $N_2O_5 + N_2 \rightarrow NO_2 + NO_3 + N_2$) increases also at high temperature (over 80 ^oC). Thus, one can conclude that the best NO_x reduction efficiency can be achieved in the order: with 10 μm water droplets, then with 100 μm water and less efficiently with no water. This may be due to the fact that smaller water droplets play a more significant role for N_2O_5 capture and compete with reaction R17. For example, with an excess of ozone (150 ppm) the NO_x oxidation efficiency can also be evaluated from the NO_2 concentration in the flue gas. Compare to the case of no water droplets (Fig. 9 (a)) where NO_2=21 ppm at 80° C or NO_2=26 ppm at 100° C, the 10 μm H_2O (Fig. 8 (e)) droplet content gives improvement in NOx oxidation i) from 67.5% to 85% at 100° C or ii) from 73.8 % at 80 °C to 85% at 100 °C. This suggests that the presence of a water spray in the reactor could substantially increase the rate of NO_x removal. However, it must be noted that it is not obviously desirable to have a mist of nitric acid in the reactor, so the balance of adverse and favorable effects has to be considered carefully.

2.8 Conclusions – gas power plant

FTIR and UV gas absorption measurements have been performed in a NO_x oxidation reactor in a large scale experiment where NO_x was oxidized by plasma-generated O_3. Reduction rates higher than 95% have been achieved for a molar ratio O_3:NO_x = 1.56. A rate equation model has been developed to assess the deNO_x chemical kinetics in the reactor under various experimental conditions (for example, different flue gas temperatures and humidity). A good agreement was found between measured and calculated values of the main species. Simulation suggests that in current experiment conditions, the deNO_x efficiency is highest for a flue gas temperature of 100 ^oC. The addition of small water spray droplets in the reactor may further improve the NO_x oxidation rate.

3 Pilot test measurements in a power plant running on biomass

3.1 Introduction

Biomass such as wood and straw are CO_2 neutral fuels which may help to reduce the greenhouse effect. The Danish resources of biomass for the production of energy are estimated to approximate 165PJ a year and only half of which are currently used

[20]. The use of biomass for production of energy is expected to keep an ascendant trend despite of its rater low caloric value. The main pollutants resulting from biofuels are nitrogen, chlorine, potassium and silicon. While potassium and chlorine are deposited on the tubes of the boiler as a salt coating (deposition that can be reduced by silicon) the main emission remains NO_x.

The current project also aimed to evaluate the use of the low temperature oxidation by ozone for a biomass power plant both in terms applicability but also for evaluating the SO_x and HCl effect on the NO_x reduction mechanism.

3.2 Chemical kinetics of NOx reduction in the presence of SOx and HCl

A gas kinetics procedure similar to that presented in paragraph 2.4 was used. The gas phase reactions included in the simulation supplementary to reactions presented in Table 1 are listed in Table 2. The solubility coefficients of SO_2, SO_3 and HCL in water are, 1.2, ∞ and 2.5×10^3, respectively.

ID	Reaction	A (cm^3 $molecule^{-1}s^{-1}$)	E_a (kcal/mol)	β	Ref
R32	SO + O3 → SO2 + O2;	4.50×10^{-12}	2.33	0	[1]
R33	SO + O2 → SO2 + O(3P);	1.6×10^{-13}	4.53	0	[1]
R34	SO + O2 → SO3;	6.1×10^{-21}	0.543	0	[1]
R35	SO2 + O3 → SO3 + O2;	3.01×10^{-12}	13.91	0.73	[1]
R36	SO2 + NO2 → SO3 + NO;	2×10^{-26}	0	0	[1]
R37	SO2 + N2O5→ SO3 + N2O4;	9.1×10^{-24}	0	0	[1]
R38	SO2 + ClO → SO3 + Cl;	4×10^{-18}	0	0	[1]
R39	SO + ClO → SO2 + Cl;	3.22×10^{-11}	0	0	[1]

Table 2 Main reactions involving SO_x.

Calculated evolutions of O_3, NO, NO_2, N_2O_5, SO, SO_2 and SO_3 concentrations in the reactor during 20 seconds after ozone injection are shown in Fig. 10 as an example, for (a) no water and (b) including 10 μm water droplets. The flue gas temperature was set to 115 °C and the input ozone to 500 ppm for a flue gas composition including, 60 ppm of SO_2, 140 ppm of NO, 10 ppm of NO_2 and 70 ppm of HCl. The hydrolysis of N_2O_5 on droplets was described in a similar way as presented in paragraph 2.6.

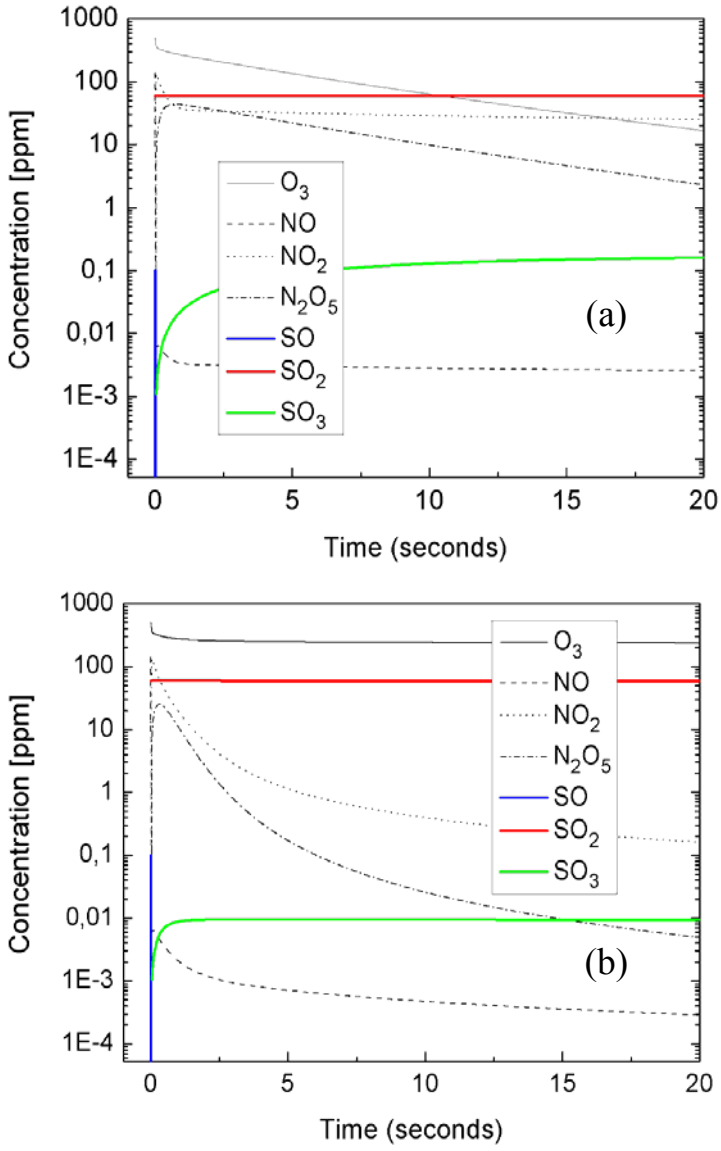

Fig. 10 Calculated evolutions of O_3, NO, NO_2, N_2O_5, SO, SO_2 and SO_3 concentrations in the reactor during 20 seconds after ozone injection, (a) no water and (b) including 10 μm water droplets.

Since the oxidation rate of SO_2 to SO_3 is too low, due to high E_a for this reaction, one cannot expect an efficient SO_x reduction by ozone despite of a good solubility of SO_3 in water. A significant oxidation of SO_2 to SO_3 can only be achieved at temperatures higher than 400°C a value that conflicts with the need to keep the working temperature below 130°C as to prevent the O_3 destruction. Moreover, N_2O_5 back reaction can also occur at high flue gas temperatures.

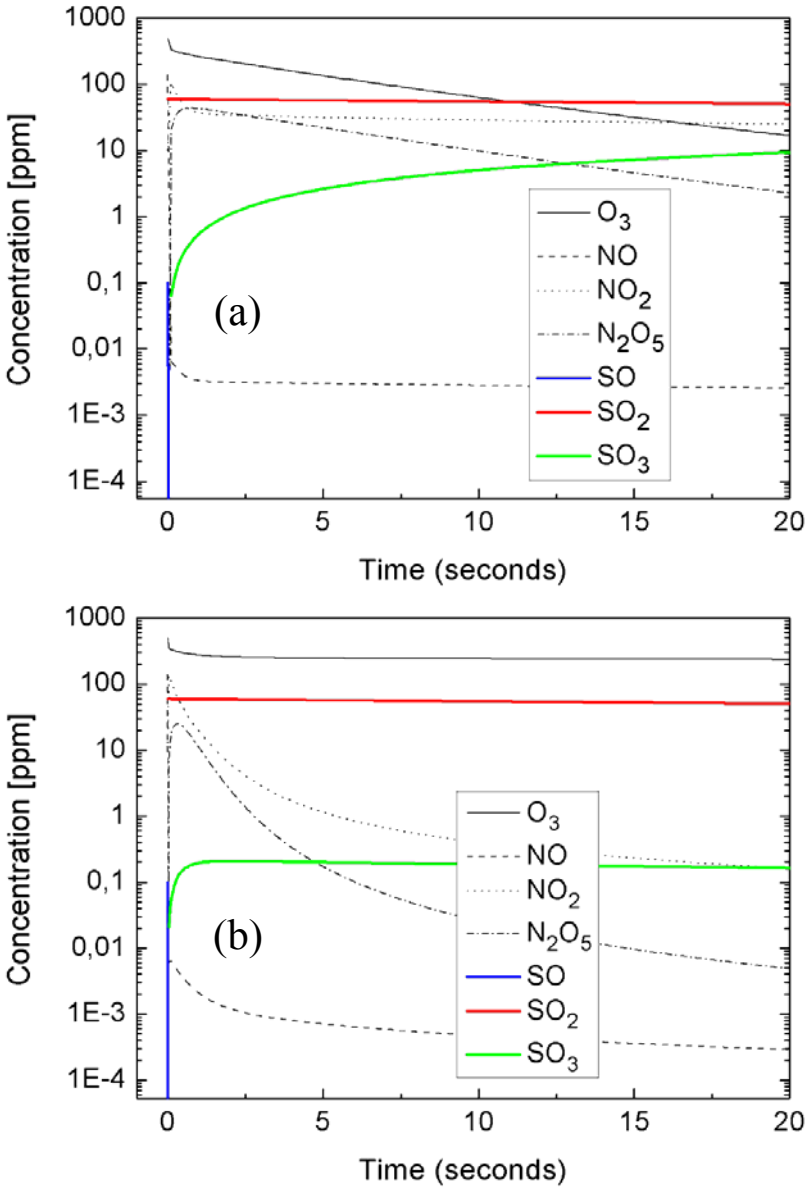

Fig. 11 Calculated evolutions of O_3, NO, NO_2, N_2O_5, SO, SO_2 and SO_3 concentrations in the reactor during 20 seconds after ozone and COl injection (100 ppm) (a) no water and (b) including 10 μm water droplets.

The evolution of simulated concentrations of different radicals in the presence of 100 ppm of ClO is presented in Fig. 11 (a) with no water and (b) with 10μm water droplets. The other input concentrations are similar with those used in Fig. 10. Except for the effect on water droplets on H_2O_5 the simulation shows that ClO will have very limited influence on NO_x and SO_x reduction.

One alternative would be to remove simultaneously SO_2 and NO by wet scrubbing using chlorine dioxine solution [21]. HCl can also be removed by wet scrubbing as shown in the following reaction,

$$2HCl+Ca(OH)_2+2H_2O \quad (12)$$

3.3 Experimental details – Haslev

The following aspects were significantly different from the measurements performed at the power plant running on natural gas in Ringsted:

- The flue gas temperature was around 115 °C (only 60° C at Ringsted);
- The NO_x level was strongly fluctuating in time, in a range from 100 ppm up to 300 ppm (the NO_x level in Ringsted was almost constant at 80 ppm);
- The inner pressure in the reactor was positive (slightly negative at Ringsted);
- Higher water vapor concentrations;
- Large content of dust particles (almost dust free combustion at Ringsted).

All these aspects needed special care for the measurement system that was severely affected by water condensation and deposition of large dust particles on the observation windows as shown in Fig. 12 (a). In order to avoid these problems the windows were flashed all the time with a low flow of dry air as shown in Fig. 12 (b).

Fig 12 (a) Measurement windows contaminated with large dust particles; (b) Mounting system for observation window including a small pipe for pouring dry air.

3.4 Experimental results and discussion

Three traces of the NO_x level recorded continuously for 15 min at time intervals larger than several hours are shown in Fig. 13. As one can see, due to unavoidable unsteady combustion of the straw, the NO_x level was fluctuating most of the time with variations larger than 100 ppm in less than one minute.

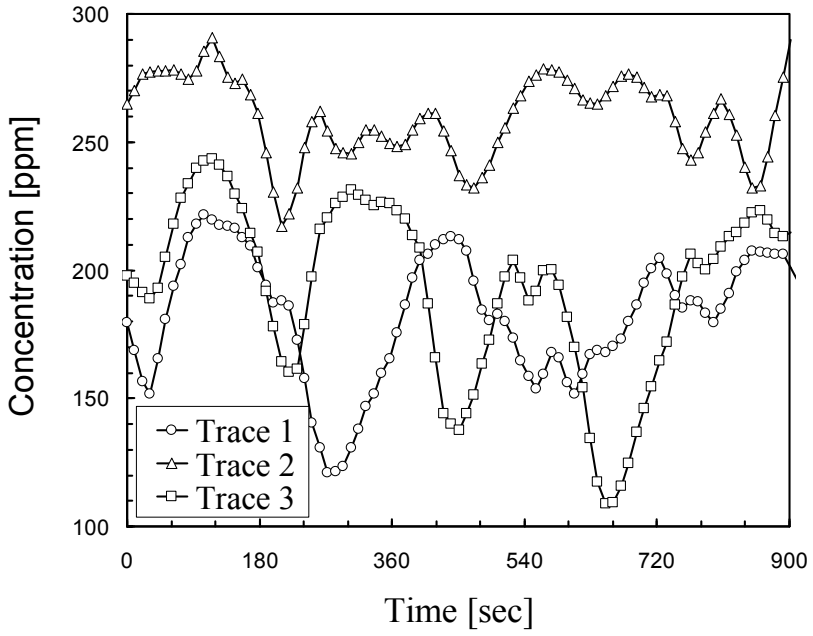

Fig. 13 Typical NO_x levels as a function of time for a biomass power plant, showing very large variation within one minute time interval.

The NO_x levels measured at the input, NOx_In, and output, NOx_Out, of the reactor with the corresponding level of ozone after the oxidation process took place, Ozone_Out, are shown in Fig. 14 for a constant input of ozone of (a) 300 g/h and (b) 500 g/h. While a NO_x reduction rate of about 50% resulted in large amounts of unused ozone correlated with low NO_x levels at that particular time, a NO_x reduction rate larger than 80% resulted in amounts of unused ozone that are unaffordable taking into consideration that the operation cost is mainly reflected in the price of the ozone.

In order to solve the problem of a time dependent NO_x level for biomass power plants a special NO_x reduction scheme was implemented. The main idea is that one can minimize the ozone loss by correlating the ozone and NO_x levels at the input of the reactor. Since the ozone generator has an internal reaction time to deliver and transport a requested amount of ozone, ΔT_{O3}, the optimization scheme can not be implemented as a direct feedback between the NO_x level at the input of the reactor and the command signal of the ozone generator. For example, the reaction time for the ozone generator used in this project is shown in Fig. 15, where the requested ozone level was incremented with 100 g/h by 3 minutes time intervals.

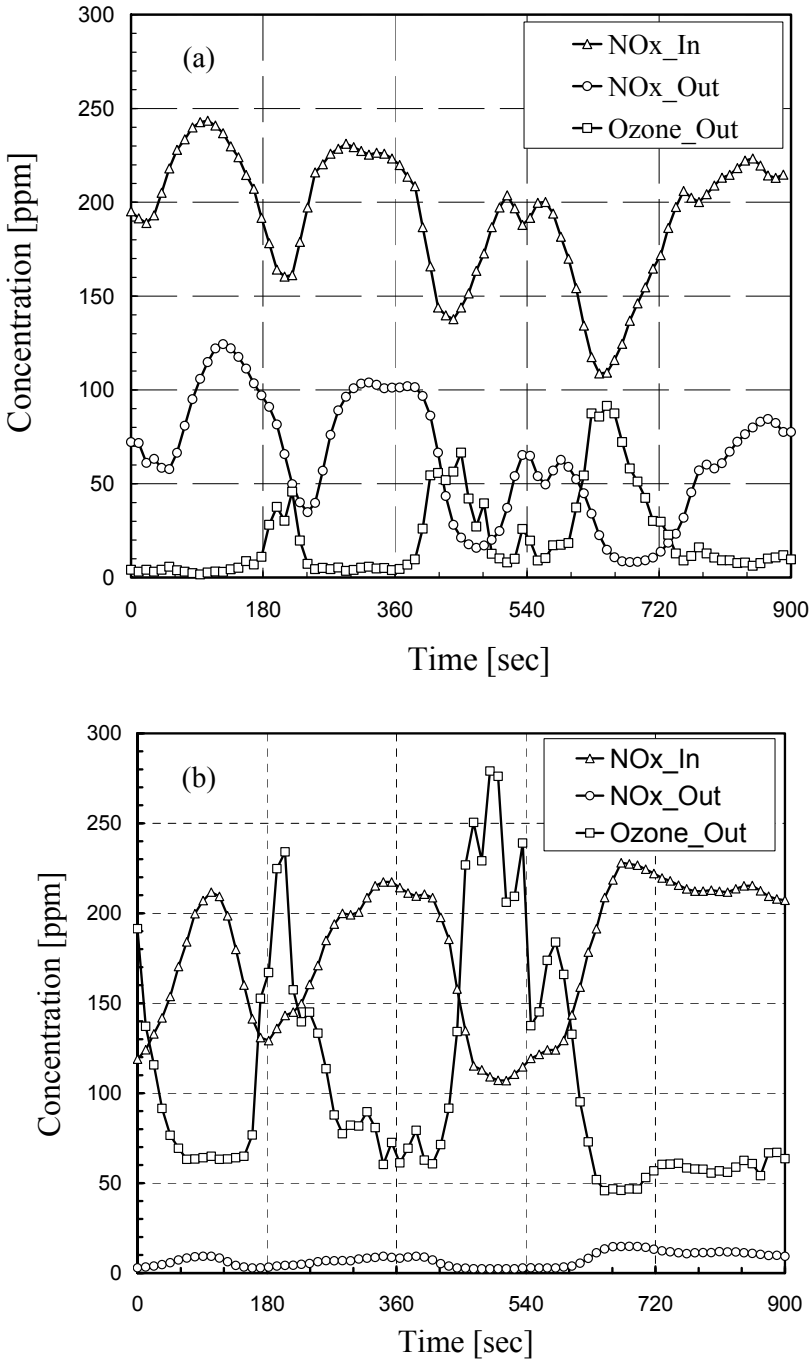

Fig. 14 NO_x levels at the input and output of the reactor with the corresponding unconsumed ozone for a constant input of ozone of (a) 300 g/h and (b) 500 g/h.

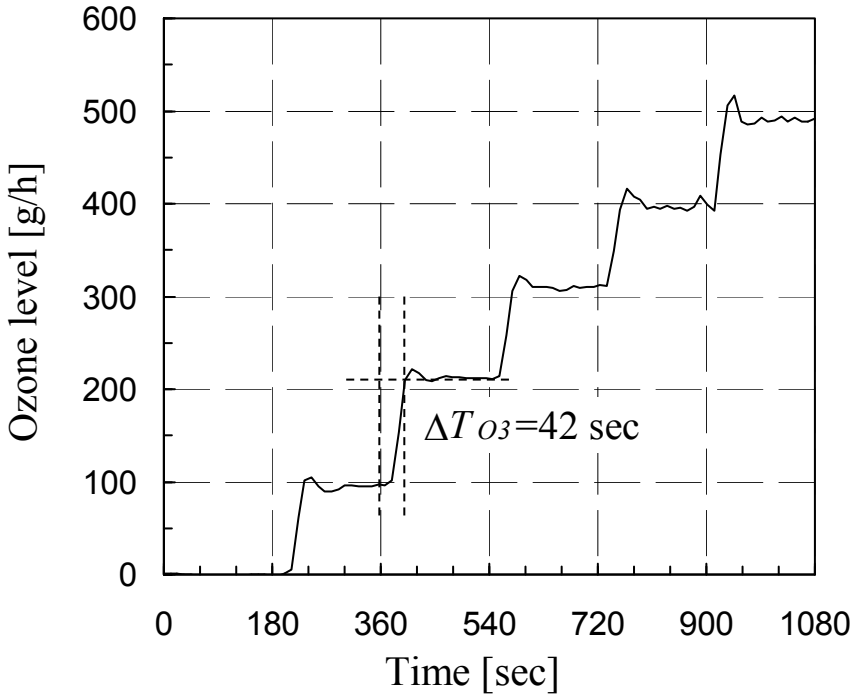

Fig. 15 Ozone levels showing an almost constant generation and transport time of about 42 seconds without respect of the delivered concentration. The ozone generator was set to change its output at equal time intervals of exactly 3 min.

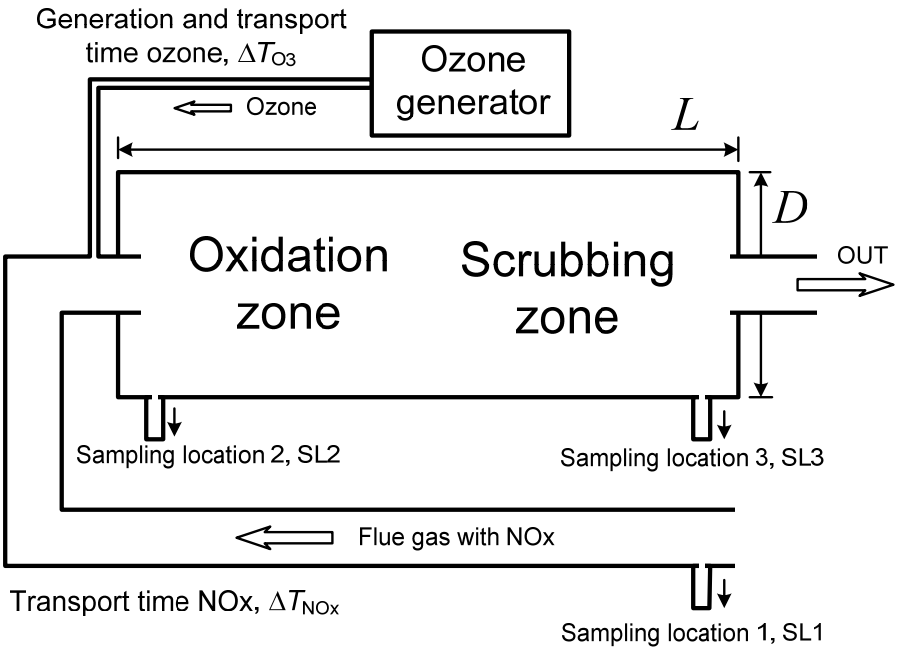

Fig. 16 Schematic of the optimization scheme. NO_x is sampled at locations SL1, SL2 and SL3 while ozone at SL2 and SL3.

This measurement shows that the generator needed about 42 seconds to adjust the ozone level to the requested value and to transport it to the entrance of the reactor. For an optimum match between the NO_x and ozone levels one needs to know the NO_x level more than 42 sec prior to the flue gas entrance in the reactor.

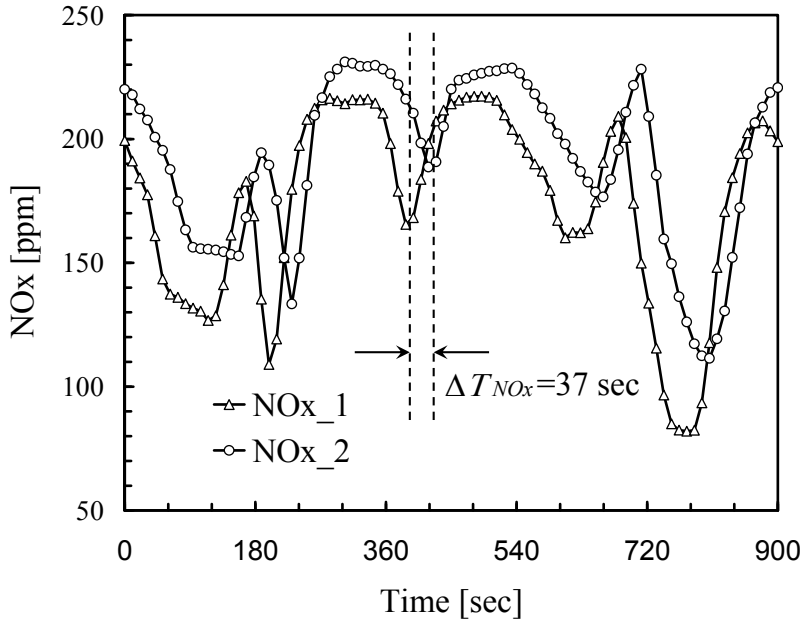

Fig. 17 NO_x levels at two locations, 1 and 2, showing that a transportation line of 25 m between provides a time delay of 37 seconds. The 10 % difference in the NO_x levels is attributed to different sensor calibration.

The implementation of such an optimization principle is shown in Fig. 16 where the oxidation and the scrubbing zones are merged schematically. SL1, SL2 and SL3 are three sampling locations where the NO_x level can be measured while the ozone level is measured only at SL2 and SL3. If ΔT_{NOx} is the transport time between SL1 and SL2 then one needs a geometric distance of about 35 m to compensate ΔT_{O3} at a gas flow of 0.9 m/sec. Since most of the power plants are using rather long evacuation lines for the flue gas, including portions of heath exchange, it makes possible to ensure ΔT_{NOx} time intervals of more than 20 seconds by placing a NO_x sensor as close as possible to the combustion zone.

The NO_x level measured at two locations situated about 25 m apart is shown in Fig. 17 from where one can deduce a transport time of 37 sec. The 10% difference in the NO_x levels can be the result of different calibration between the power plant sensor and DGC's NO_x detection system. The very good correlation between the shapes of the two signals proves that one can use the NO_x level measured at a location prior the reactor entrance to compensate the reaction and transport time for

ozone. In practice the ozone generator can be placed just a few meters from the oxidation reactor, so that it is possible to assume that the ΔT_{O3} is mainly the reaction time of the generator.

In order to test this optimization scheme the rental time for the equipment was extended with two weeks. However, this time interval was not enough for a complete implementation, so that, the optimization scheme was implemented only partially in the sense that we could compensate only time fluctuations larger than one 30 sec.

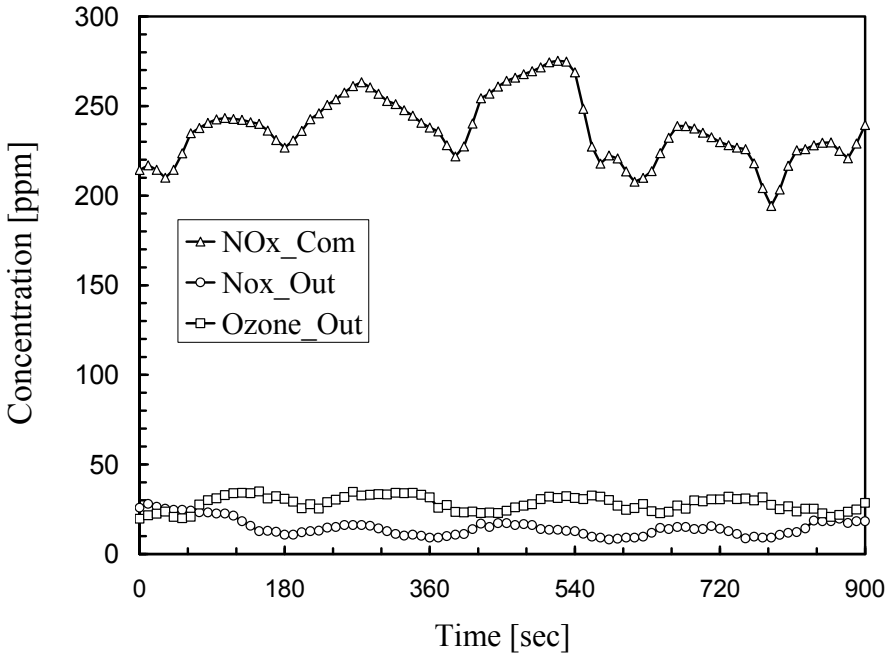

Fig. 18 NO_x level commanding the ozone generator, NOx_Com, and NOx and ozone levels after the scrubber, NOx_Out and Ozone_Out, respectively.

Fig. 18 presents with NOx_Com the NO_x level used to command the ozone level in the ozone generator, and NOx_OUT and Ozone_OUT the NO_x and ozone levels after the scrubber. A NO_x reduction rate higher than 85% obtained at the same time with a low level of unconsumed ozone proves the applicability of this new optimization scheme which was not previously used in research or direct implementations for NO_x reduction by ozone oxidation.

3.5 Conclusions – biomass power plant

NO_x reduction by ozone oxidation is applicable for biomass power plants. However, due to large fluctuations in the NO_x level within time intervals of a few minutes a special optimization scheme ensuring an efficient use of ozone is required. Such

optimization has been developed and partially implemented. The oxidation rate of SO_2 to soluble SO_3 by ozone is too low at temperatures below 130 °C. Higher operation temperatures are not applicable due to significant ozone destruction. SO_x and HCl have a very small effect on NO_x reduction by ozone.

4 References

[1] Orlandini I and Riedel U, J Phy. D: Appl Phys 2000;33:2467-2474.

[2] Chen J P and Yang R T, Appl Catal A 1992;80:135-148.

[3] Lyon R K, US Patent No. 3900554 (1975).

[4] Nam C M, Gibbs B M, Proc Combust Inst 2000;28:1203-9.

[5] Jarvis J B, Naresh A T D, Suchak J, $LoTO_x$ process flexibility and multi-pollutant control capability. Presented at the combined power plant air pollutant control mega symposium, Washington, DC, May 19-22, 2003.

[6] Mukkavilli S, Lee C K, Varghese K, and Tavlarides L L, IEEE Trans Plasma Sci 1988;16:652-660.

[7] Dinelli G, Civitano L, and Rea M, IEEE Trans Ind Appl 1990;26:535-541.

[8] Chakrabarti A, Mizuno A, Shimizu K, Massuoka T, and Furuta S, IEEE Trans Ind Appl 1995;31:500-6.

[9] Yamamoto T, Yang C L, Kravets Z, and Kravets M, IEEE Trans Ind Appl 2000;36:923-7.

[10] Chang S J, Loay P C, Nagai K, Yoshioka T, Aoki S, Moezawa A, IEEE Trans Ind Appl 1996;32:131-7.

[11] Martin D I, Ighigeanu D I, Mateescu E N, Craciun G D, Calinescu I I, Iovu H M, and Marin G G, IEEE Trans Ind Appl 2004;40:41-52.

[12] Ferrel R, Pollut. Engr. 2000;32:50-3.

[13] Yoshioka Y, Sano K and Teshima K, J Adv Oxid Technol 2003;6:143-9.

[14] Eliasson B and Kogelschatz U, IEEE Trans Plasma Sci 1991;19:309-323.

[15] Using Non-Thermal Plasma to control air polluants, Report EPA-456/R-05-001 United States Environmental Protection Agency, Feb. 2005
http://www.epa.gov/ttn/catc/dir1/fnonthrm.pdf

[16] Kirkegaard P, Bjergbakke E, and Olsen J V, *Risø-R-1085 (ed.2) (EN)*, 1 (2006).

[17] NIST database, http://kinetics.nist.gov/

[18] Voegele A F, Tautermann CS, Loerting T, and Liedl K R, Phys.Chem.Chem.Phys. 2003;5:487-495.

[19] Van Doren J M, Watson L R, Davidovits P, Worsnop D R, Zahniser M S, and Kolb C E J Phys Chem 1990;94:3265-69.

[20] Bioenergy for electricity and heat – experiences from biomass-fired CHP plants in Denmark, published by DONG Energy, 2007
[21] D.S. Jin et al., *Journal of Hazardous Materials B* 135 (2006) 412.

Risø DTU is the National Laboratory for Sustainable Energy. Our research focuses on development of energy technologies and systems with minimal effect on climate, and contributes to innovation, education and policy. Risø has large experimental facilities and interdisciplinary research environments, and includes the national centre for nuclear technologies.

Risø DTU
National Laboratory for Sustainable Energy
Technical University of Denmark

Frederiksborgvej 399
PO Box 49
DK-4000 Roskilde
Denmark
Phone +45 4677 4677
Fax +45 4677 5688

www.risoe.dtu.dk